Coniferous Forest Leaf Area Index Estimation along the Oregon Transect Using Compact Airborne Spectrographic Imager Data

Peng Gong, Ruiliang Pu, and John R. Miller

Abstract

Leaf area index (LAI) is an important structural variable for quantitative analysis of the energy and mass exchange characteristics of a terrestrial ecosystem. Previous research on estimating forest LAI by remote sensing is limited to the use of conventional multispectral data. Methods used for LAI estimation involved primarily simple statistical relationships between LAI and vegetation indices (VI) derived from remote sensing data.

In this paper, the potentials of an imaging spectrometer, the Compact Airborne Spectrographic Imager (CASI), have been studied for coniferous forest LAI estimation using three types of modeling techniques: univariate regression, multiple regression, and vegetation-index (VI) based LAI estimation. Four study sites have been selected along a forest transect in Oregon. LAI measurements were collected from these study sites. CASI data of two imaging modes — spatial and spectral — had been calibrated and corrected. The relationships between the LAI measurements and the corrected CASI data were then explored.

Results indicate that the CASI data acquired with the two imaging modes have similar accuracies for LAI prediction. All three LAI estimation methods resulted in LAIs with reasonably low root-mean-squared errors (RMSEs). The use of the normalized difference vegetation index (NDVI) produced more accurate LAI estimates than did the use of channel ratio for the univariate regression and the VI-based LAI prediction methods. For the univariate regression, a non-linear hyperbola relationship between the LAI and the NDVI was the most appropriate for LAI estimation. In this study, the VI-based LAI estimation method has proven to be simple to use and effective.

P. Gong was with the Department of Geomatics Engineering, The University of Calgary, Calgary, Alberta T2N 1N4, Canada, and is currently with the Department of Environmental Science, Policy, and Management, University of California at Berkeley, Berkeley, CA 94720.

R. Pu is with the Department of Forestry, Nanjing Forestry University, Nanjing 210037, P.R. China.

J.R. Miller is with the Earth-Observations Laboratory, The Institute for Space and Terrestrial Science, Department of Physics, York University, 4850 Keele Street, North York, Ontario M3J 3K1, Canada.

Introduction

Leaf area index (LAI), the projected leaf surface area per unit ground area, is an important structural variable for quantifying the energy and mass exchange characteristics of a terrestrial ecosystem (Lathrop and Pierce, 1991; Herwitz *et al.*, 1990; Spanner *et al.*, 1990a; Nemani and Running, 1989; Running *et al.*, 1989; Curran and Williamson, 1987; Asrar *et al.*, 1984). It is probably the most useful parameter to be extracted from remote sensing data for crop yield prediction and crop stress assessment in agricultural studies, and for estimation of forest canopy characteristics and determination of forest exchange rates of carbon dioxide, water, and oxygen. For instance, the relationships between LAI and vegetation indices derived from various kinds of remote sensing data were studied in order to estimate a number of agronomic variables (Curran, 1983; Asrar *et al.*, 1984; Baret *et al.*, 1989; Batista and Rudorff, 1990; Clevers, 1991). That a strong correlation between LAI and vegetation indices exists was reported in those studies. Running *et al.* (1989) used forest LAI as an important variable in a forest biogeochemical (FOREST-BGC) model to map regional forest evapotranspiration and photosynthesis by coupling satellite sensor data with ecosystem simulation. Based on an assumption that an equilibrium exists between climate, soil water-holding capacity, and maximum leaf area in water-limited coniferous forest ecosystems, Nemani and Running (1989) developed a quantitative relationship among the three factors. This relationship allows the prediction of either equilibrium LAI or soil water-holding capacity if the other is known. In addition, the determination of LAI by remote sensing would also allow calculation of canopy photosynthesis and evapotranspiration over a global scale at a relevant time interval (Gutman, 1991; Spanner *et al.*, 1990b).

Running *et al.* (1986) attempted to estimate the LAI of coniferous forests using an airborne Thematic Mapper Simulator (TMS) data by establishing a relationship between the forest LAI and the ratio of a near infrared (NIR) band to a red (R) band. The LAI of temperate coniferous forests across a regional gradient was found to be related to the ratio of NIR to R TMS spectral bands (Peterson *et al.*, 1987). Using multitemporal Advanced Very High Resolution Radiometer (AVHRR) data, Spanner *et al.* (1990a) derived the normalized differ-

Photogrammetric Engineering & Remote Sensing,
Vol. 61, No. 9, September 1995, pp. 1107–1117.

0099-1112/95/6109–1107$3.00/0

TABLE 1. TREE SPECIES, NUMBER OF LAI MEASUREMENTS, AND AVAILABLE CASI IMAGERY AT EACH STUDY SITE

Tree Species	No. of LAI	Dates and Resolution (m) of CASI Data	
		Spatial-mode	Spectral-mode
Red Alder, Western Hemlock, Sitka Spruce (Site 1)	13	16 May (1.12×2.46)	16 May (2.23×2.46)
Douglas Fir (Site 2)	11	16 May (2.23×2.46)	16 May (2.23×9.45)
Western Hemlock, Douglas Fir Red Alder (Site 3)	11	15 May (2.23×2.46)	15 May (2.23×9.45)
Ponderosa Pine (Site 5)	8	20 May (1.71×2.5)	20 May (2.23×9.45)

ence vegetation index (NDVI) for large area LAI studies. They found that there was an asymtotic relationship between maximum July AVHRR NDVI data and the seasonal LAI maximum of coniferous forests of the western United States while the winter minimum NDVI values could not be explained entirely by phenological reduction of LAI probably due to some abiotic factors. After examining the relationships between LAI of temperate coniferous forests and Landsat Thematic Mapper (TM) spectral bands, ratios, and transforms, Spanner *et al.* (1990b) found that LAI estimation was affected by canopy closure, understory vegetation, and background reflectance. LAI changes of closed-canopy pine plantations in central Massachusetts were evaluated using Landsat TM data (Herwitz *et al.*, 1990) and it was concluded that the TM data might provide a more reliable guide to changes in the LAI of closed canopy plantations at local scales than field measurements based on allometric equations. Seasonal LAI in slash pine was estimated based on the NDVI derived from Landsat TM data of three different seasons for the study of forest seasonal dynamics (Curran *et al.*, 1992). A discrepancy between LAI values derived from ground-based canopy transmittance and those from Landsat TM NIR/R ratios has been noted in Lathrop and Pierce (1991). The differences are especially evident at low overstory LAI levels where differential background reflectance becomes important. A spectral derivative method was used to suppress the effects of background soil on tree spectra leading to improved correlation between LAI values measured from a low canopy closure ponderosa pine stand and data from the Compact Airborne Spectrographic Imager (CASI) (Gong *et al.*, 1992).

Most previous studies on forest LAI estimation using remote sensing methods are primarily limited to the use of conventional multispectral data with a selected number of relatively broad spectral bands. Most of these studies have focused on finding a linear or non-linear relationship between LAI and various vegetation indices (VI) derived from remote sensing data. In a recent study, multitemporal remotely sensed data collected on three different airborne platforms over a transect of coniferous forest stands in Oregon were analyzed with respect to seasonal LAI (Spanner *et al.*, 1994). Four different sensors were used including the broad spectral-band TMS and three narrow spectral-band high spectral resolution sensors: the CASI, the Airborne Visible/Infrared Imaging Spectrometer (AVIRIS), and a Spectron SE590 spectroradiometer. Strong logarithmic relationships were observed between seasonal maximum and minimum LAI and the NIR/R for all these sensors (R^2 = 0.82 to 0.97). The correlation was examined at the forest stand level for all six study sites selected in the Oregon Transect Ecosystem Research (OTTER) project (Peterson and Waring, 1994).

In this study, efforts were focused on estimating LAI, at a level of spatial scale smaller than that in Spanner *et al.* (1994), using data collected from a CASI instrument over four of the six OTTER coniferous forest sites. CASI acquires images in two modes, spatial and spectral, with very high spectral resolution (Anger *et al.*, 1990). The objectives of this paper are

- to determine what technique is more appropriate for coniferous LAI estimation using CASI data, and
- to compare the effectiveness of the spatial and spectral imaging modes of CASI for LAI estimation.

The Study Sites

The six OTTER study sites are located along a temperature-moisture gradient across west-central Oregon, called the Oregon transect. They are Cascade Head (Site 1), Waring's Woods (Site 2), Scio (Site 3), Santiam Pass (Site 4), Metolius River (Site 5), and Juniper (Site 6) (Peterson and Waring, 1994). The transect cuts across seven vegetation zones from the western coast to the eastern high desert of Oregon. The distributions of various zones and locations of study sites as well as coniferous species composition of each zone were described in detail in Gholz (1982). The LAI variation (from > 10 to < 1) across this transect is controlled by both temperature and moisture (Runyan *et al.*, 1994). Canopy closure is greater than 90 percent for some of the western stands, and is less than 50 percent for some of the eastern stands. The understory vegetation along the transect consists of highly varying proportions of ferns, shrubs, and various grasses, with little exposed rock or soil along the first four study sites. Sites 5 and 6 have about 10 to 30 percent of soil exposure. In this study, only four sites — Sites 1, 2, 3, and 5 — were used. Major tree species for the four study sites are listed in Table 1.

Data Collection and Preprocessing

Field LAI Measurements

An LAI-2000 Plant Canopy Analyzer (PCA) was used in the field to measure forest LAI. The operation instructions for the LAI instrument were followed carefully to make sure that the measured LAIs were within 10 percent of the mean values with a 0.95 confidence level (LI-COR Inc., 1990). From 15 May to 22 May, 1991, a total of 58 LAI measurements were taken by the authors at the six study sites. Out of these, 52 LAI measurements were collected under coniferous forest stands. The time involved in taking one LAI measurement ranged from a few minutes to half an hour depending on the accessibility of the site and the weather condition. The numbers of LAI measurements for four of these study sites are

listed in Table 1. Each LAI measurement represents an average of five to ten point PCA readings which were taken in an area between 40 and 100 m^2. The locations of LAI measurements in each study site were selected based on the canopy closure, age of stands, and nutrient level so as to make them representative of the variability in the site. Separated at least 10 m away from each other, the LAI measurements were considered as independent samples. The exact locations from which the LAI measurements were taken were marked on color infrared aerial photographs. These have been used as references for spectral data extraction from CASI images. A conversion factor has been used for each forest species to transform readings from an LAI-2000 PCA to LAI values (LI-COR Inc., 1990).

CASI Data Acquisition and Calibration

CASI is a relatively portable imaging spectrometer developed for use on board small aircraft or in laboratories. Due to the limitation of data recording rate, CASI is operated in two modes, a spatial mode and a spectral mode. In the spatial mode, the CASI acquires spatial images with each line having the full spatial resolution (512 pixels) and with up to 18 spectral channels. In addition, the spectral band widths, number, and ground cell resolutions are programmable in the spatial mode. In the spectral mode, the CASI generates images in which each pixel has a complete spectrum from approximately 417 nm to 927 nm in 288 bands, with an average spectral bandwidth of 1.76 nm and a spectral resolution of the spectral mode of CASI is approximately 3.5 nm. In this case, each image line has only 39 pixels, resulting in an image covering only stripes of areas along an aircraft flight track. The viewing direction along the swath can be selected interactively by the operator.

CASI data were acquired during the period of 16 to 21 May 1991 as part of the OTTER multiplatform airborne remote sensing campaign. Due to poor weather conditions or pilot misjudgement, LAI measurement locations from only four of the six OTTER study sites can be clearly identified from the data acquired (Table 1). The flight heights for these CASI data range from 900 m to 1800 m. Eight spectral channels were selected for the spatial mode according to the characteristics of a general vegetation spectral reflectance curve. These spectral channels are located at spectral regions including the blue, the inflection point of the blue-green slope, the green peak, the red well, the inflection point of the red edge, the red-edge shoulder, and two near-infrared bands (Table 2). Although the CASI spectral-mode data were calibrated using the CASI manufacturer's parameters, the resultant radiance values for each image pixel are noisy. The noise came from two major sources: the specific atmospheric absorption features and the system errors. The first noise source has been suppressed using a radiance-to-reflectance conversion procedure described later. The second noise source has strong effects on the radiance values collected at wavelengths longer than 800 nm. Thus, radiance values at spectral bands whose wavelengths are longer than 800 nm have not been used in this study. The lack of spectral bands with wavelengths ranging from 800 nm to 1100 nm was not a problem in this study because there were enough spectral bands covering the shoulder of a tree spectral curve in both the spectral- and spatial-mode CASI imagery.

All the spatial-mode and spectral-mode CASI images have been checked to identify LAI measurement locations by referring to the marked aerial color-infrared photographs. As a result, 30 LAI measurement locations have been identified from the four study sites for the spatial-mode images while 28 LAI measurement sites have been located on the spectral-mode CASI images. Spectral data were then extracted from both the spatial-mode and the spectral-mode CASI images. Because of different sky conditions among different study sites, it is impossible to use radiance data directly from CASI images for LAI estimation. For this reason, the CASI data were converted from radiance to reflectance using simple linear relationships between reflectance measured from pseudo-invariant targets for each scene and the corresponding radiance from the CASI images. Ground reflectance measurements were taken using a SPECTRON SE-590 radiometer during the same field study period. The pseudo-invariant targets include roads, gravel pits, roof tops, and parking lots (Freemantle *et al.*, 1992).

The extracted spectral-mode CASI data have been further processed using a band-merging method. Every five successive spectral bands have been merged to form a new channel. This resulted in 43 merged channels with their centers ranging from 421.2 nm to 794.4 nm and each of which has a band width of approximately 8.8 nm (Table 2). There are two reasons for spectral band merging for the spectral-mode CASI data. First, band merging grouped originally narrow bands to suppress the noise noted above. Second, the number of channels has to be reduced in order to make better use of a multiple regression algorithm for LAI estimation. As explained later, the piece-wise multiple regression method will produce inflated LAI estimation results if the number of channels to be used as independent variables is much greater than the number of LAI measurements.

Model Developments

In order to estimate LAI from CASI data, the exact forms of LAI as a function of CASI data have to be established. Three types of models have been used in this study. In each model, the LAI of coniferous forests was defined as the dependent variable while spectral reflectance of each channel, its transforms such as its logarithmic transform, and two types of vegetation indices (e.g., NDVI =(NIR − R)/(NIR + R) and RVI = NIR/R) were defined as independent variable(s). On the image each LAI location corresponds to approximately 10 to 20 pixels. The average spectral reflectances for each LAI location were taken from the images. The three types of models are described below.

Univariate Linear and Nonlinear Prediction Models

A total of seven univariate LAI prediction models were used. They include

- a simple linear function, $Y=a + bX$;
- a power function, $Y = aX^b$;
- an exponential function, $Y=a\cdot\exp(bX)$;
- another exponential function, $Y=a\cdot\exp(b/X)$;
- a logarithmic function, $Y=a+b\cdot LOG(X)$;
- a hyperbola function, $Y=1/(a+b/X)$; and
- an **S**-model curve, $Y=1/(a+b\cdot\exp(-X))$;

where Y represents the LAI to be predicted, a and b are regression coefficients, and X denotes the independent variable. Candidates for X included the eight bands in the spatial-mode and the 43 merged channels in the spectral-mode and many ratios and NDVIs. The purpose was to select an optimal model that produced the best goodness of fit (GOF) for LAI estimation using CASI data (Xu, 1988). Those ra-

TABLE 2. CHANNEL AND MERGED-CHANNEL WAVELENGTHS (NM) OF THE CASI IMAGES USED IN THIS STUDY

Spatial-Mode		Spectral-Mode									
CH#	λ	MCH#	λ	MCH#	λ	MCH#	λ	MCH#	λ	MCH#	λ
1	440.3	1	421.2	10	499.6	19	578.8	28	658.7	37	739
2	497	2	429.9	11	508.4	20	587.6	29	667.6	38	747.9
3	551.4	3	438.5	12	517.1	21	596.5	30	676.5	39	756.8
4	679.2	4	447.2	13	525.9	22	605.4	31	685.4	40	765.8
5	711.3	5	455.9	14	534.7	23	614.2	32	694.3	41	774.7
6	738.1	6	464.6	15	543.5	24	623.1	33	703.2	42	783.7
7	747.9	7	473.4	16	552.3	25	632	34	712.1	43	794.4
8	787.3	8	482.1	17	561.1	26	640.9	35	721.1		
		9	490.8	18	570	27	649.8	36	730		

Note: CH# = channel number of the spatial-mode CASI data
MCH# = merged-channel number of the spectral-mode CASI data
λ = central wavelength (nm).

tios and NDVIs producing relatively high GOFs are presented in Tables 3, 4, and 5.

VI-Based LAI Estimation

After examining the potentials and limits of vegetation indices for LAI and APAR (absorbed photosynthetic active radiance) estimation, Baret and Guyot (1991) published a model in which the variation of VI, as a function of LAI, can be expressed by a modified Beer's law: i.e.,

$$VI = VI_\infty + (VI_g - VI_\infty) \cdot exp\ (-K_{VI} \cdot LAI) \quad (1)$$

where VI_g is the vegetation index corresponding to that of the bare soil, VI_∞ is the asymptotic value of VI infinity (practically, this limit can always be reached when LAI is greater than 8.0), and K_{VI} is an attenuation coefficient. For the purpose of this study, Equation 1 has been rearranged in order to estimate LAI: i.e.,

$$LAI = -\ \mathrm{Ln}\ \left(\frac{VI - VI_\infty}{VI_g - VI_\infty}\right) / K_{VI}. \quad (2)$$

In this approach, VI_∞ was specified with the maximum value appearing in this study, while VI_g was obtained by averaging vegetation indices on the bare soil from the four study sites.

Piece-Wise Multiple Regression

A forward piece-wise regression procedure (Tang, 1984) was employed to determine channel combinations that were most strongly associated with the LAI. The input to the piece-wise regression procedure is the LAI values measured in the field and spectral reflectances at each channel. The output is a series of multivariate linear equations which are different from each other by the number of spectral channels involved, and the goodness of fit (GOF) and the standard deviation associated with each equation. In this method, the regression equation is developed by successive insertion of a predictor variable (e.g., a spectral channel) into the equation based on the ranking of the partial correlations of all variables that are not selected with the dependent variable (LAI). The final regression equation, after running the piece-wise program, can be expressed in the following form:

$$Y = b_0 + b_1 x_1 + b_2 x_2 + \cdots + b_k x_k \quad (3)$$

where X_i represents the ith predictor (independent) variable, usually channel reflectance or channel logarithmic reflectance, Y denotes the predicted LAI, and b_i is the ith regression coefficient (b_0 is a constant) having the "best" GOF. The accuracy of LAI estimation by the univariate and multiple regression models was evaluated using the root-mean-squared error (RMSE).

Results and Discussion

Correlating LAIs with Spatial-Mode CASI Data

Univariate Correlations between the LAIs and the Spatial-Mode CASI Data

As mentioned above, spectral data corresponding to 30 LAI measurements were extracted from the spatial-mode CASI data for the four sites. The distributions of the 30 LAI measurement locations are ten for site 1, six for site 2, six for site 3, and eight for site 5. The highest GOFs were obtained from those derivative data consisting of channel ratios and NDVIs calculated from a combination of the NIR channels and the red channel. The linear and highest non-linear GOFs for the eight single channels and the six sets of derivative data with the highest GOFs are listed in Table 3. It is interesting to note that the highest non-linear GOFs were all obtained using the hyperbola model. The S-model curve fitting consistently resulted in the second best GOFs, while the two models based on power functions produced the third best GOFs. From a

TABLE 3. GOODNESS OF FIT DERIVED FROM LINEAR AND NONLINEAR REGRESSIONS BETWEEN LAI AND CHANNEL, LAI AND NDVI, OR LAI AND RVI OBTAINED USING THE SPATIAL-MODE CASI DATA (N = 30)

Code	Channel Types	Linear Fitting (R^2)	Nonlinear Fitting (R^2) Hyperbola Model	Nonlinear Fitting (R^2) Exponential Model
1	ch 1 (440.3 nm)	0.25	0.40	
2	ch 2 (497.0 nm)	0.36	0.58	
3	ch 3 (551.4 nm)	0.11	0.21	
4	ch 4 (679.2 nm)	0.46	0.72	
5	ch 5 (711.3 nm)	0.01	0.06	
6	ch 6 (738.1 nm)	0.36	0.39	
7	ch 7 (747.9 nm)	0.42	0.46	
8	ch 8 (787.3 nm)	0.49	0.55	
9	(ch6−ch4)/(ch6+ch4)	0.65	0.86	0.80
10	(ch7−ch4)/(ch7+ch4)	0.65	0.87	0.81
11	(ch8−ch4)/(ch8+ch4)*	0.65	0.87	0.81
12	ch6/ch4	0.70	0.87	0.80
13	ch7/ch4	0.71	0.87	0.80
14	ch8/ch4	0.72	0.88	0.80

*the highest among codes 9, 10, 11

TABLE 4. ROOT-MEAN-SQUARE ERRORS (RMSE), GOODNESS OF FIT, AND MEAN ATTENUATION COEFFICIENTS (K) OBTAINED FROM DIFFERENT ANALYSIS METHODS WITH THE SPATIAL-MODE CASI DATA

Independent Variables in Equations	RMSE	R^2	K/Sk*
Piece-wise Regression Analysis			
LOG(ch1),LOG(ch2),LOG(ch3),LOG(ch8)	0.982	0.83†	
LOG(ch1),LOG(ch3),LOG(ch8)	0.836	0.81†	
LOG(ch6),LOG(ch8)	0.873	0.73†	
Univariate Regression			
ch8/ch4	1.697	0.88	
ch7/ch4	1.729	0.87	
ch6/ch4	1.727	0.87	
(ch8−ch4)/(ch8+ch4)	1.117	0.86	
(ch7−ch4)/(ch7+ch4)	1.110	0.86	
(ch6−ch4)(ch6+ch4)	1.117	0.85	
VI-based LAI Estimation			
(ch8−ch4)/(ch8+ch4)	1.172		0.420/0.119
(ch7−ch4)/(ch7+ch4)	1.206		0.376/0.110
(ch6−ch4)/(ch6+ch4)	1.227		0.367/0.109

*: K/Sk=mean attenuation coefficient/standard deviation of K; †: significant at p=0.01.

pure model fitting point of view, as indicated in Table 3, it seems that hyperbola functions are more appropriate to use as compared to the more widely used power functions (e.g., those used in Peterson *et al.* (1987), Spanner *et al.* (1990b), and Spanner *et al.* (1993)). Among the three near-infrared channels, channel 8 and channel 7 have higher GOFs with the LAIs than does channel 6. This is because channel 6 is located at the red-edge shoulder where the higher near-infrared reflecting behavior of a tree species is still affected by the absorption property at the red wavelength region. This is particularly true for channel 5, located at the inflection point of the red edge. The mediating effect of the NIR and the red spectral bands has made the GOFs between channel 5 and the LAIs approach 0.

The highest single-channel non-linear GOF with the LAIs was achieved at channel 4, the red spectral region. According to general conclusions of other researchers that the higher the APAR of vegetation, the lower is the spectral reflectance of vegetation at the red band, the stronger relationship between channel 4 and the LAIs seems to be reasonable because more vigorous vegetation is likely leading to higher LAI. In the non-linear relationships, both channel ratio and NDVI applied to the three NIR channels and the red channel resulted in high GOFs with the minimum of 0.86 obtained from correlating the LAIs with the NDVI derived from channel 6 and channel 4 (Figure 1). These agree well with other researcher's findings that the NDVI and the ratio vegetation index have strong relationships with LAI, although power functions and linear models were used in other studies (e.g., Peterson *et al.*, 1987; Spanner *et al.*, 1990a; Curran and Williamson, 1992). From Figures 1a and 1b, it can be seen that the channel 4 reflectance and the NDVI saturate when LAI is slightly greater than 4 while, from Figure 1c, it can be seen that the channel 8 and channel 4 ratio saturates as LAI is over 6. The linear relations between NDVI and LAI and between the channel ratio and LAI, as indicated by GOFs, are 0.650 and 0.717, respectively. It seems that the channel ratio is more sensitive to LAI change than to the NDVI.

LAI Estimation with Spatial-Mode CASI Data

LAIs of coniferous forests were predicted using three techniques: univariate regression, piece-wise multivariate regression, and the VI-based estimation. For each prediction technique, the 30 samples were divided into two groups: predicting and testing. The predicting group consisted of 20 samples while the remaining ten were used as test samples. The predicting group was used in coefficient estimation to establish the LAI prediction equations, while the test group was used to calculate the root-mean-square errors (RMSEs). The division of predicting sample and test sample was made randomly so as to have the test sample as representative to the total sample as possible. The variable types used in LAI predicting equations, accuracies of the predictions measured by RMSEs, and GOFs (R^2) are listed in Table 4. While the RMSEs were obtained from test samples, the GOFs were calculated from the predicting samples at the same time as the predicting equations were derived.

It can be seen from Table 4 that the only comparable measure for all the three types of LAI estimation techniques is the RMSE. The lowest estimation errors have been achieved with the use of piece-wise regression. After comparing the effectiveness of multiple regression using different types of variables (e.g., original reflectance, transforms, etc.), it was found that the logarithmic value of channel reflectance had the best relationship to LAIs. Therefore, in the multiple regression analysis, each of spectral reflectance was transformed into its logarithmic counterpart. For the univariate regression case, even though some of the channel ratios had high GOFs in relation to LAIs, they produced greater RMSEs as compared to NDVIs (Table 4). The univariate regression

TABLE 5. ROOT-MEAN-SQUARE ERRORS (RMSE), GOODNESS OF FIT, AND MEAN ATTENUATION COEFFICIENTS (K) OBTAINED FROM DIFFERENT ANALYSIS METHODS WITH CASI DATA IN SPECTRAL MODE

Independent Variables in Equations	RMSE	R^2	K/Sk*
Piece-wise Regression Analysis			
LOG(mch2),LOG(mch3),LOG(mch14),LOG(mch34)	1.405	0.87†	
LOG(mch3),LOG(mch14),LOG(mch34)	1.652	0.83†	
LOG(mch3),LOG(mch14)	1.642	0.78†	
Univariate Regression			
(mch40−mch22)/(mch40+mch22)	0.764	0.97	
(mch40−mch25)/(mch40+mch25)	0.848	0.97	
(mch43−mch29)/(mch43+mch29)	1.151	0.97	
VI-based LAI Estimation			
(mch40−mch22)/(mch40+mch22)	1.079		0.297/0.060
(mch40−mch25)/(mch40+mch25)	1.033		0.328/0.066
(mch43−mch29)/(mch43+mch29)	1.218		0.439/0.130

*: K/Sk=mean attenuation coefficient/standard deviation of K; †: significant at p=0.01.

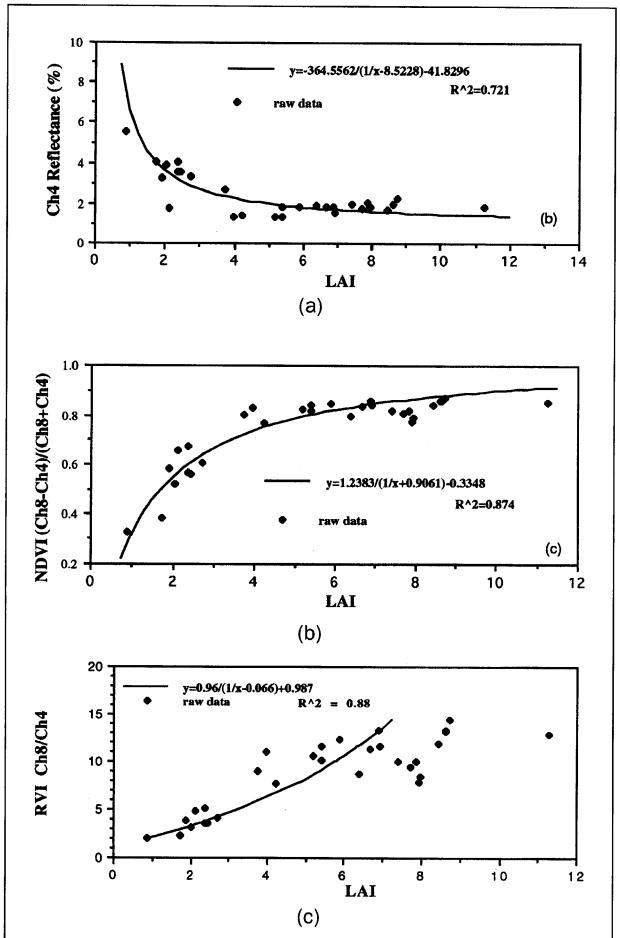

Figure 1. Correlations between LAI measurements and (a) CH4, (b) NDVI (CH8 − CH4)/(CH8 + CH4), and (c) RVI CH8/CH4 using the spatial-mode CASI data. CH4 and CH8 correspond to 679.2 nm and 787.3 nm, respectively.

method based on NDVIs has produced slightly smaller errors than the VI-based LAI estimation.

For the VI-based LAI estimation method, the mean attenuation coefficient (K) was calculated directly from Equation 2. This was done by first calculating each K_i using the corresponding LAI_i and VI_i, and then the K_i were averaged to form the K to be used in the LAI prediction. S_k is the standard deviation of K. The GOFs obtained using the multiple regression method are significant at the 0.99 probability level. Among the results obtained from each of the three techniques, all the errors are relatively small when compared to the magnitude of the LAIs.

The field measured LAI values have been compared with those predicted ones for the multiple regression, univariate regression, and the VI-based model, respectively (Figures 2, 3, and 4). It is evident when compared with Figure 2 that data points in Figures 3 and 4 tend to have a larger scattering pattern, indicating a poorer agreement between the predicted and measured LAIs. It is interesting to note that in every figure a larger discrepancy between the predicted LAIs and the LAI measurements can be observed as the LAI value exceeds approximately 6.0. From a computational point of view, the VI-based LAI estimation is the simplest. On the other hand, the multiple regression algorithm is more flexible. It does not require channels to be in the red and NIR spectral regions.

Correlating LAIs with Spectral-Mode CASI Data

Univariate Correlation Analysis between LAIs and Merged Channels

GOFs obtained from both the linear correlation and the best non-linear correlation have been plotted versus the central wavelengths of the merged channels (Figure 5). Most of the visible channels have resulted in surprisingly high GOFs

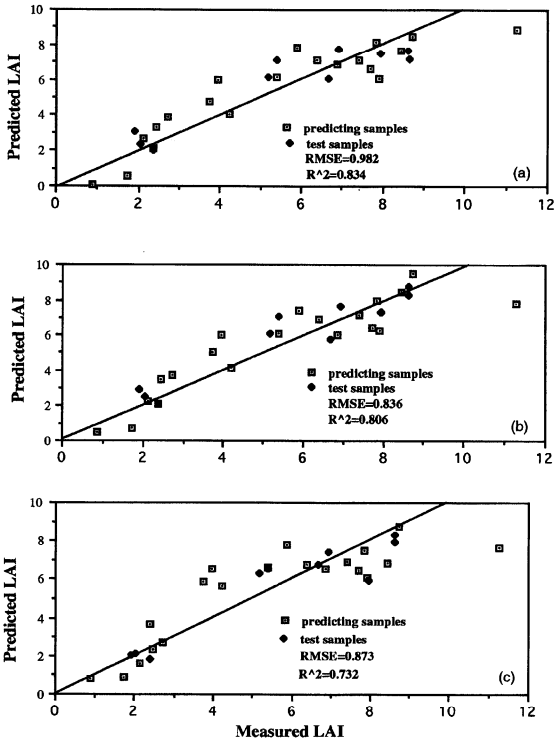

Figure 2. Measured LAIs compared with predicted LAIs using the piece-wise regression with CASI spatial data. Predicted LAIs were obtained from both the 20 predicting samples used for setting up the predicting equation and the ten test samples. (a) Predicted with four channels corresponding to 440.3 nm, 497.0 nm, 551.4 nm, and 787.3 nm, respectively; (b) predicted with three channels corresponding to 440.3 nm, 551.4 nm, and 787.3 nm, respectively; and (c) predicted with two channels corresponding to 738.1 nm and 787.3 nm, respectively.

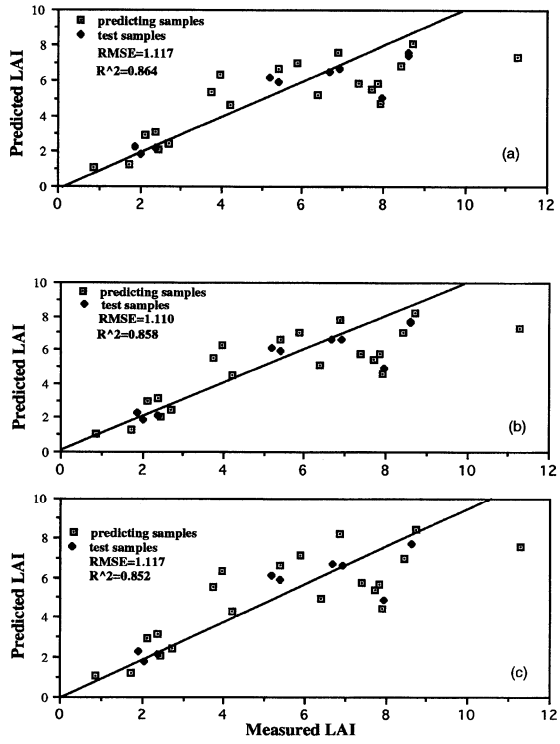

Figure 3. Measured LAIs compared with predicted LAIs using the univariate regression with spatial-mode CASI data. Predicted LAIs were obtained from both the 20 predicting samples used for setting up the predicting equation and the ten test samples. (a) Predicted with NDVI between NIR CH8 and R CH4; (b) predicted with NDVI between NIR CH7 and R CH4; and (c) predicted with NDVI between NIR CH6 and R CH4. Channel wavelengths can be found in Table 2.

while the NIR channels have lead to very low GOFs. A number of factors might have contributed to low GOFs among the NIR channels. First, the spectral-mode data had relatively large pixel sizes and only covered a portion of the study area in a systematic manner. These made it difficult to precisely locate the LAI measurement sites. In other words, location mismatching between ground and the spectral-mode CASI images could introduce errors. While little variation may occur in the visible bands because of the low spectral reflectances of tree stands, in the near infrared bands the sensor may be very sensitive to the large pixel-averaging effects and possible misplacement of LAI sites. Second, sensor calibration errors may also contribute to the low GOFs in the NIR bands. Such errors are related to (1) the relatively poor internal data calibration in the NIR bands, (2) the inconsistency of the narrow band wavelengths between the CASI and the Spectron Engineering 590 field spectroradiometer used to collect spectra for pseudo-invariant targets, and (3) the temporal differences caused different weather conditions during the period of CASI and the field spectroradiometer data acquisition across the four study sites.

LAI Estimation Using Spectral-Mode CASI Data

Similar to the LAI prediction analysis with the spatial-mode CASI data, the three LAI estimation techniques were also applied to the spectral-mode CASI data. The most accurate prediction results in terms of the lowest RMSEs have been listed in Table 5. A total of only 28 LAI measurement locations have been found from the spectral-mode images. Again, 20 samples were divided into the predicting group while the remaining eight were used as test sample. "Mch" was used to represent merged channels. Similar to the use of the spatial-mode CASI data, the logarithm of original channel reflectance had a greater power of LAI prediction than the original reflectance and various channel combinations for the multiple regression case.

Different from the spatial-mode's case, however, the NIR channels of the spectral-mode CASI data made little contribu-

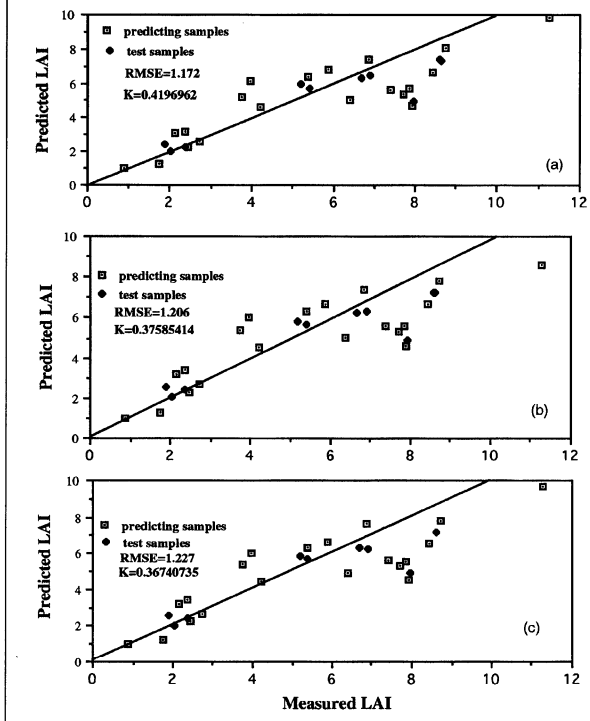

Figure 4. Measured LAIs compared with predicted LAIs using the VI-based LAI estimation method with CASI spatial data. Predicted LAIs were calculated by using both the 20 predicting samples used to derive the average attenuation coefficient (K) and the ten test samples. (a) Predicted with NDVI between NIR CH8 and R CH4; (b) predicted with NDVI between NIR CH7 and R CH4; and (c) predicted with NDVI between NIR CH6 and R CH4. Channel wavelengths can be found in Table 2.

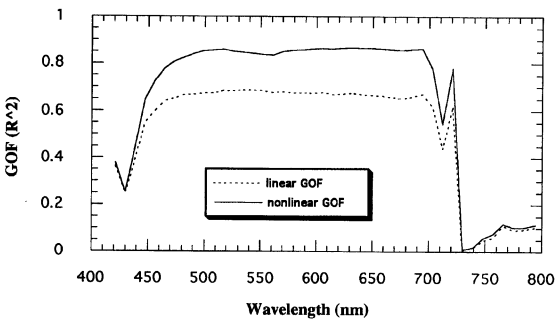

Figure 5. Goodness of fit obtained from linear and non-linear regressions between LAI and merged channels.

tion to LAI prediction with multiple regression possibly due to the reasons mentioned in the previous section (Table 5). For the univariate regression analysis and the VI-based LAI estimation methods, NDVIs have shown better performance than have other variables such as channel ratios and individual merged channels. In combination with what has been found from the use of spatial-mode CASI data, NDVI as a measure of LAI seems to be more robust than channel ratios. The NDVI is less sensitive to variations in location, viewing angle, and lighting conditions when compared with the NIR channels because the NIR channels acquired from different sites and at different times of the day produced very low GOFs.

The RMSEs for the piece-wise regression method are the highest among the three methods (Table 5). By comparing the RMSEs obtained from the univariate regression and VI-based LAI estimation methods, we see that the univariate method has lower RMSEs than does the VI-based method. When comparing GOFs derived from the piece-wise method with univariate regression, the GOFs of the latter are considerably higher than those of the former. The predicted LAIs and the measured LAIs are compared for each of the three methods (Figures 6, 7, and 8). Again, better agreements can be found when LAI values are less than 6.0. This is consistent with what Figures 2, 3, and 4 show.

A Comparison of the Two CASI Imaging Modes for LAI Estimation

The results obtained by correlating each individual channel (or merged channel) with measured LAIs show that in the visible region the spectral-mode CASI data have a considerably stronger correlation with LAIs than do the spatial-mode CASI data. For instance, for the spectral-mode CASI data, the GOFs obtained using the merged channel 30 (676 nm) of the spectral-mode data are 0.65 and 0.86 using a linear and a non-linear hyperbola model, respectively (see Figure 5). On the other hand, the highest linear and non-linear GOFs for the spatial-mode data obtained from the use of channel 4 (679 nm) are 0.46 and 0.72, respectively. At the NIR region, however, the GOFs obtained with the spectral-mode data are much lower than those obtained with the spatial-mode data.

By comparing the RMSEs in Table 4 with those in Table 5, the LAI prediction accuracies are better with the spatial-mode data than those with the spectral-mode data for the multiple regression method. On the other hand, most of the prediction accuracies obtained from using the spectral-mode data are higher than those obtained from using the spatial-mode data for the univariate regression and the VI-based LAI estimation method.

The same trend held when the practical effectiveness of the three LAI estimation methods were further validated. LAI prediction equations were used to estimate the LAIs of coniferous forests in a broader spatial scale for three selected study sites (Sites 2, 3, and 5) using the available CASI images. An average radiance value was extracted from every spectral channel for each study site. These radiances were then converted to spectral reflectances. Having been converted to logarithmic values or transformed into NDVIs, they were used as inputs to the LAI prediction equations. Table 6 summarizes the LAI estimation results as compared to ground-based LAI estimates for each selected study site (ground-based LAIs were provided by R. Waring). A relative error, defined as the ratio of the standard deviation (between the remote sensing estimates and ground-based estimates) and the average

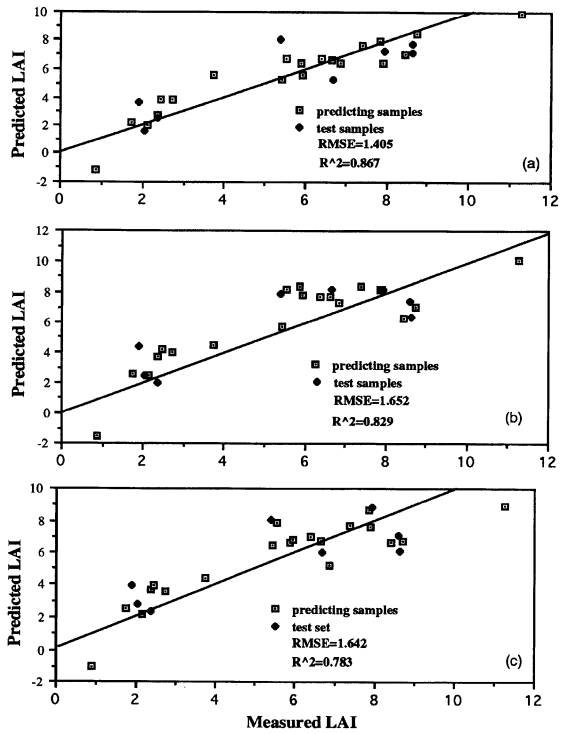

Figure 6. Measured LAIs compared with predicted LAIs using the piece-wise regression with CASI spectral data. Predicted LAIs were obtained from both the 20 predicting samples used for setting up the predicting equation and the eight test samples. (a) Predicted with four channels corresponding to 429.9 nm, 438.5 nm, 534.7 nm, and 712.1 nm, respectively; (b) predicted with three channels corresponding to 438.5 nm, 534.7 nm, and 712.1 nm, respectively; and (c) predicted with two channels corresponding to 438.5 nm and 534.7 nm, respectively.

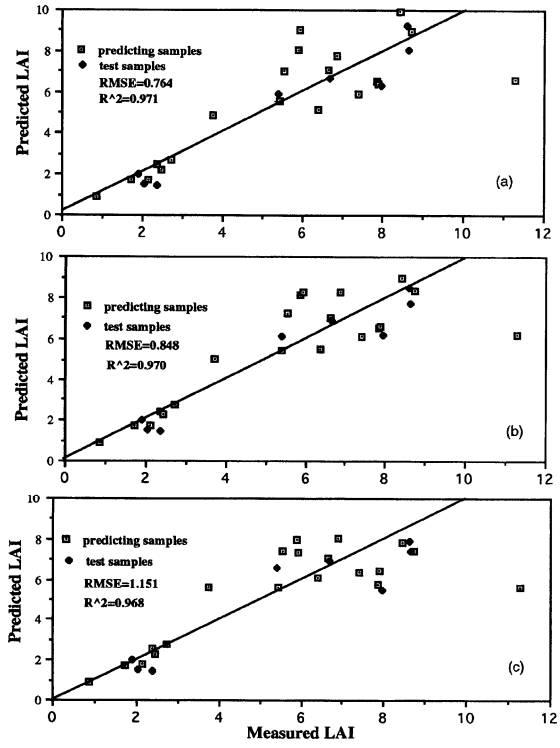

Figure 7. Measured LAIs compared with predicted LAIs using the univariate regression with CASI spectral data. Predicted LAIs were obtained from both the 20 predicting samples used for setting up the predicting equation and the eight test samples. (a) Predicted with NDVI between NIR MCH40 (765.8 nm) and R MCH22 (605.4 nm); (b) predicted with NDVI between NIR MCH40 (765.8 nm) and R MCH25 (632.0 nm); and (c) predicted with NDVI between NIR MCH43 (794.4 nm) and R MCH29 (667.6 nm).

ground-based estimates, was calculated for each method (Table 6). The relative errors range from 11 percent to 17 percent. In this comparison, results from the VI-based LAI estimation method have shown the best agreement with the ground-based LAI estimates, while the multiple regression and the univariate regression ranked the second and the third, respectively. The spectral-mode CASI data have resulted in slightly better LAI estimates than have the spatial-mode data. The LAI values in Table 6 were estimated using the following equations:

For the spatial mode,

Model I: LAI = − 8.089 − 59.124•Log(CH6) + 65.555•Log(CH8),

Model II: LAI = 1/(− 0.9061 + 1.2383/(NDVI + 0.3348)), and

Model III: $LAI = -Ln\left(\frac{NDVI - 0.9}{0.01925 - 0.9}\right)/0.416$

where NDVI = (CH8 − CH4)/(CH8 + CH4).

For the spectral mode,

Model I: LAI = 4.620 + 4.334•Log(MCH2) − 4.908•Log(MCH3) − 1.570•Log(MCH14) + 1.655•Log(MCH34),

Model II: LAI = 1/(− 0.7970 + 1.0824/(NDVI + 0.3924)), and

Model III: $LAI = -Ln\left(\frac{NDVI - 0.85}{0.03616 - 0.85}\right)/0.3187$

where NDVI = (MCH40 - MCH25)/(MCH40 + MCH25).

Conclusions

One of the objectives of this study was to evaluate three methods — piece-wise multiple regression, univariate regression, and the vegetation-index-based method — for LAI estimation using two different modes of CASI data: the spatial and spectral modes. The piece-wise multiple regression method resulted in lower RMSE prediction errors as com-

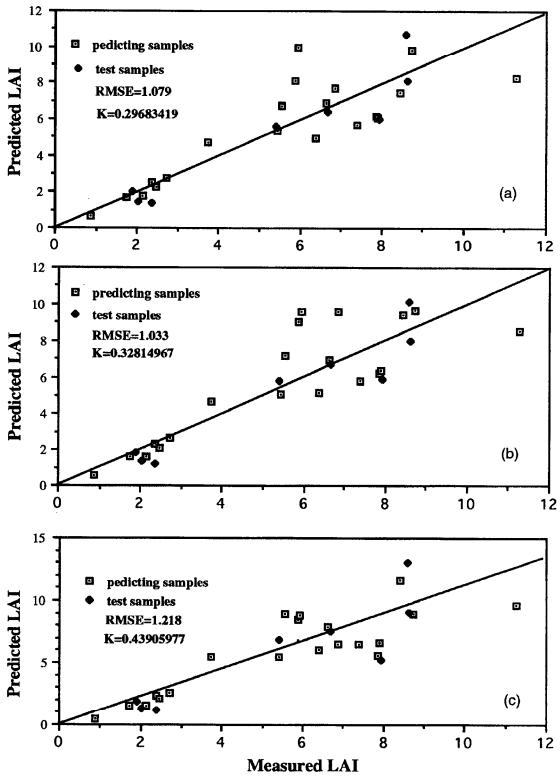

Figure 8. Measured LAIs compared with predicted LAIs using the VI-based LAI estimation method with CASI spectral data. Predicted LAIs were calculated by using both the 20 predicting samples used to derive the average attenuation coefficient (*K*) and the eight test samples. (a) Predicted with NDVI between NIR MCH40 (765.8 nm) and R MCH22 (605.4 nm); (b) predicted with NDVI between NIR MCH40 (765.8 nm) and R MCH25 (632.0 nm); and (a) predicted with NDVI between NIR MCH43 (794.4 nm) and R MCH29 (667.6 nm).

TABLE 6. CROSS VALIDATION OF PREDICTED LAI USING THREE TECHNIQUES: PIECE-WISE (I), UNIVARIATE REGRESSION (II), AND VI-BASED LAI ESTIMATION (III) WITH CASI DATA*

Study Area	G.B.LAI	CASI LAI Estimation					
		Spatial-mode			Spectral-mode		
		I	II	III	I	II	III
site 2	6.33	6.42	6.24	6.43	6.45	6.75	6.54
site 3C	7.23	8.77	5.62	5.77	7.82	8.66	8.17
site 3IF	8.46	9.03	9.14	8.67	8.46	8.84	8.34
site 5C	0.8	1.08	1.06	1.05	2.17	1.49	1.48
site 5F	1.8	1.18	1.20	1.15	1.77	1.42	1.37
Average relative error		0.16	0.17	0.15	0.14	0.16	0.12

Note: G.B.LAI - ground-based LAI measurement; C-control study area; F-fertilized study area; and IF-intensively fertilized study area
*These ground-based LAI measurements were provided by Richard Waring. They were collected from the study site level which is completely different from the other LAI measurements used in the rest of this study.

pared to the univariate regression and the VI-based LAI estimation methods using the spatial-mode CASI data. However, it produced the largest RMSEs among the three methods when CASI spectral-mode data were used. For both the spectral and spatial-mode CASI data, the use of logarithmic reflectance in the multiple regression method produced lower RMSEs than did the use of raw channel reflectance. The advantage of the piece-wise multiple regression method is its flexibility in the use of spectral bands. Instead of using the near-infrared (NIR) and red (R) spectral bands as in the other two methods, the multiple regression method can be used to estimate LAI reasonably well with only two spectral bands: merged channels 3 (438.5 nm) and 14 (534.7 nm) which are in the blue and green spectral regions, respectively (see Table 5). We recommend that the multiple regression method be used to discover new relationships between LAI and spectral reflectances derived from remote sensing imagery. Because this method is rooted purely on a statistical basis, further studies may be carried out to identify the biophysical reasons behind those discovered relationships.

In this study, NDVI starts to saturate before LAI reaches 6. Linear correlations indicated that channel ratio is more correlated with LAI. However, NDVI appeared to be a non-linear better estimator of LAI than channel ratio for the univariate regression and the VI-based LAI estimation methods. For the univariate regression, a non-linear hyperbola relationship between the LAI and the NDVI was the most appropriate for LAI estimation. The VI-based LAI estimation method has proven to be simple to use and effective. Further studies are required to verify these two models in different forest environments.

Although the spatial- and spectral-mode CASI data produced similar LAI estimation results using the three methods, we recommend the use of the spatial-mode CASI data for LAI estimation. With spectral-mode CASI data, it is difficult to locate LAI measurement sites and that, in turn, may affect the final LAI estimation results. However, the multiple regression method should be further evaluated for LAI estimation using high spectral resolution data other than the spectral-mode CASI data.

Acknowledgments

The authors are grateful to their colleagues, Jim Freemantle, Yoshio Awaya, Mike Belanger, Mike Spanner, and Lee Johnson, who helped during the field data collection and the CASI data processing stages of this study. Ground-based leaf area index data were provided by Richard Waring from the Oregon State University. Paul Curran has kindly provided very helpful comments on a draft copy of this paper. This research was funded by a Centre of Excellence grant from the Province of Ontario to the Institute for Space and Terrestrial Science and NSERC Research Grants to P. Gong and J.R. Miller. Three anonymous reviewers contributed to improve the presentation of this paper.

References

Anger, C.D., S.K. Babey, and R.J. Adamson, 1990. A New Approach to Imaging Spectrometry, *Proceedings of SPIE*, 1298:72-86.

Asrar, G., M. Fuchs, E.T. Kanemasu, and J.L. Hatfield, 1984. Estimating Absorbed Photosynthetic Radiation and Leaf Area Index from Spectral Reflectance in Wheat, *Agronomy Journal*, 76:300-306.

Baret, F., and G. Guyot, 1991. Potentials and Limits of Vegetation Indices for LAI and APAR Assessment, *Remote Sensing of Environment*, 35:161-173.

Baret, F., G. Guyot, and D.J. Major, 1989. Crop Biomass Evaluation Using Radiometric Measurements, *Photogrammetria*, 43:241-256.

Batista, G.T., and B.F.T. Rudorff, 1990. Spectral Response of Soybeans by Field Radiometry, *ISPRS Journal of Photogrammetry and Remote Sensing*, 45:111-121.

Card, D.H., D.L. Peterson, and P.A. Matson, 1988. Prediction of Leaf Chemistry by Use of Visible and Near Infrared Reflectance Spectroscopy, *Remote Sensing of Environment*, 26:123-147.

Clevers, J.G.P.W., 1991. Application of the NDVI in Estimating LAI at the Generative Stage of Barley, *ISPRS Journal of Photogrammetry and Remote Sensing*, 46:37-47.

Curran, P.J., 1983. Multispectral Remote Sensing for the Estimation of Green Leaf Area Index, *Phil. Trans. R. Soc. Lond. A*, 309:257-270.

Curran, P.J., and H.D. Williamson, 1987. GLAI Estimation Using Measurements of Red, Near Infrared, and Middle Infrared Radiance, *Photogrammetric Engineering & Remote Sensing*, 53(2): 181-186.

Curran, P.J., J.L. Dungan, and H.L. Gholz, 1992. Seasonal LAI in Slash Pine Estimated with Landsat TM, *Remote Sensing of Environment*, 39:3-13.

Freemantle, J.R., R. Pu, and J.R. Miller, 1992. Calibration of Imaging Spectrometer Data to Reflectance Using Pseudo-Invariant Features, *Proceedings of the 14th Canadian Symposium on Remote Sensing*, Toronto, Ontario, 1-4 June, pp. 452-455.

Gholz, H.L., 1982. Environmental Limits on Above Ground Net Primary Production, Leaf Area, and Biomass in Vegetation Zones of the Pacific Northwest, *Ecology*, 63:469-481.

Gong, P., R. Pu, and J.R. Miller, 1992. Correlating Leaf Area Index of Ponderosa Pine with Hyperspectral CASI Data, *Canadian Journal of Remote Sensing*. 18:275-282.

Gutman, G.G., 1991. Vegetation Indices from AVHRR: An Update and Future Prospects, *Remote Sensing of Environment*, 35:121-136.

Herwitz, S.R., D.L. Peterson, and J.R. Eastman, 1990. Thematic Mapper Detection of Changes in the Leaf Area of Closed Canopy Pine Plantations in Central Massachusetts, *Remote Sensing of Environment*, 29:129-140.

LAI-2000 Plant Canopy Analyzer, 1990. *Instruction and Manual*, LI-COR Inc.

Lathrop, R.G., Jr., and L.L. Pierce, 1991. Ground-Based Canopy Transmittance and Satellite Remotely Sensed Measurements for Estimation of Coniferous Forest Canopy Structure, *Remote Sensing of Environment*, 36:179-188.

Miller, J.R., E.W. Hare, and J. Wu, 1990. Quantitative Characterization of the Vegetation Red Edge Reflectance. 1. An Inverted-Gaussian Reflectance Model, *International Journal of Remote Sensing,* 11(10):1775-1795.

Nemani, R.R., and S.W. Running, 1989. Testing a Theoretical Climate-Soil-Leaf Area Hydrologic Equilibrium of Forests Using Satellite Data and Ecosystem Simulation, *Agricultural and Forest Meteorology,* 44:245-260.

Peterson, D.L., M.A. Spanner, S.W. Running, and K.B. Teuber, 1987. Relationship of Thematic Mapper Simulator Data to Leaf Area Index of Temperate Coniferous Forests, *Remote Sensing of Environment,* 22:323-341.

Peterson, D.L., J.D. Aber, D.A. Matson, D.H. Card, N. Swanberg, C. Wessman, and M. Spanner, 1988. Remote Sensing of Forest Canopy and Leaf Biochemical Contents, *Remote Sensing of Environment,* 24:85-108.

Peterson, D.L., and R.H. Waring, 1994. Overview of the Oregon Transect Ecosystem Research Project, *Ecological Applications,* 4(2): 211-225.

Running, S.W., D.L. Peterson, M.A. Spanner, and K.B. Teuber, 1986. Remote Sensing of Coniferous Forest Leaf Area, *Ecology,* 67(1): 273-276.

Running, S.W., R.R. Nemani, D.L. Peterson, L.E. Band, D.F. Potts, L.L. Pierce, and M.A. Spanner, 1989. Mapping Regional Forest Evapotranspiration and Photosynthesis by Coupling Satellite Data with Ecosystem Simulation, *Ecology,* 70(4):1090-1101.

Runyon, J., R.H. Waring, S.N. Goward, and J.M. Welles, 1994. Environmental Limits on Net Primary Production and Light-use Efficiency across the Oregon Transect, *Ecological Application,* 4(2):226-237.

Spanner, M.A., L. Johnson, J. Miller, R. McCreight, J. Freemantle, J. Runyon, and P. Gong, 1994. Remote Sensing of Seasonal Leaf Area Index across the Oregon Transect, *Ecological Applications,* 4(2):258-271.

Spanner, M.A., L.L. Pierce, S.W. Running, and D.L. Peterson, 1990a. The Seasonality of AVHRR Data of Temperate Coniferous Forests: Relationship with Leaf Area Index, *Remote Sensing of Environment,* 33:97-112.

Spanner, M.A., L.L. Pierce, D.L. Peterson, and S.W. Running, 1990b. Remote Sensing of Temperate Coniferous Forest Leaf Area Index, The Influence of Canopy Closure, Understory Vegetation and Background Reflectance, *International Journal of Remote Sensing,* 11(1):95-111.

Tang, S., 1984. *Multivariate Statistical Analysis,* Forestry Press of China (in Chinese).

Wessman, C.A., J.D. Aber, and D.L. Peterson, 1989. An Evaluation of Imaging Spectrometry for Estimating Forest Canopy Chemistry, *International Journal of Remote Sensing,* 10(8):1293-1316.

Xu, Y., 1988. *Computer Application Package to IBM-PC/XT (0520) Series,* Coal Industry Press (in Chinese).

(Received 11 August 1993; revised and accepted 1 February 1994; revised 4 April 1994)

Peng Gong

Peng Gong, B.Sc., M.Sc. (Nanjing, China), Ph.D. (Waterloo, Canada), is an assistant professor at the University of California at Berkeley. He was a Project Scientist between 1990 - 1991 at the Earth-Observations Laboratory, Institute for Space and Terrestrial Science, North York, Ontario, Canada. From 1991 to 1994, he was Assistant Professor of Geomatics Engineering, The University of Calgary, Canada. Interested in remote sensing and GIS, he is a winner of two ASPRS best paper awards in 1993. He is the 1993-94 President of the Association of Chinese Professionals in GIS (Abroad) and a member of ASPRS, IEEE, and the Canadian Society of Remote Sensing.

Ruiliang Pu

Ruiliang Pu, B.Sc., M.Sc. (Nanjing Forestry University, China), has been a lecturer in the Department of Forestry, Nanjing Forestry University, China, since 1985. In 1990 and 1991, he was a visiting scholar at the Earth-Observations Laboratory, Institute for Space and Terrestrial Science, Ontario, Canada. His research interests are in forest ecological modeling, forest inventory, and remote sensing.

John R. Miller

John R. Miller received a B.E. (Physics) at the University of Saskatchewan (Saskatoon) in 1963. He earned both M.Sc. (1966) and Ph.D. (1969) degrees in Space Physics from the same university studying the aurora borealis using rocket-borne radiometers. He then spent 2 years on a Postdoctoral Fellowship at the Herzberg Institute at the National Research Council in Ottawa. In 1971 he went to work as a Project Scientist at York University and obtained a faculty appointment in 1972. He is currently Professor of Physics & Astronomy at York University and is Co-Director of the Earth Observations Laboratory of the Institute for Space and Terrestrial Science. His remote sensing research interests have included atmospheric correction and interpretation of water color reflectance and canopy reflectance. Over the past 6 years his primary focus has been on the application of reflectance spectroscopic techniques in remote sensing using imaging spectrometers.